Int J Wireless Inf Networks (2012) 19:219–228
DOI 10.1007/s10776-012-0176-2

Characteristic and Modeling of Human Body Motions for Body Area Network Applications

Ruijun Fu · Yunxing Ye · Kaveh Pahlavan

Received: 13 January 2012 / Accepted: 14 May 2012 / Published online: 6 July 2012

Abstract Many current and future medical devices are wearable and human body is used as a carrier for wireless communication, which implies human body to be a crucial part of the transmission medium in body area networks (BANs). In order to understand the propagation characteristics around human body, the statistical model is derived for communication links in the medical implant communication service band, industrial scientific medical band and ultra-wideband based on the narrowband measurement. The channel model of diffracting components around human body were different from one scenario to another. Moreover, second order statistics, including level crossing rate and fade duration, are presented for each scenario to evaluate the link quality and outage performance for on-body to on-body scenario. Using a network analyzer, Doppler spread spectrum in frequency domain and coherence time in time domain from temporal variations of human body movements are also analyzed from diverse perspectives. Additionally, the shape of Doppler spread spectrum is fitted to describe the relationship of power and frequency. The proposed on-body to on-body channel model for human body motions can be used to better design wireless network protocols for BANs.

Keywords Body area networks (BANs) · Propagation channel · First-order statistical distribution · Level crossing rate · Fade duration · Doppler spread · RMS Doppler spread · Doppler spread spectrum · Coherence time

R. Fu (✉) · Y. Ye · K. Pahlavan
Department of Electrical and Computer Engineering, Worcester Polytechnic Institute, Worcester, MA, United States
e-mail: ruijunfu@gmail.com

1 Introduction

Rapid growth in low power integrated circuits and wireless communication has made the medical detection with miniaturized sensors come true. Body area network, which connects these wireless devices to human body, has gained considerable popularity in medical care applications [4]. These wearable and swallowable medical sensors could continuously monitor health parameters in real time and send to a central device such as smart phones. IEEE 802.16.5 Task Group 6 is officially working on standardization of BANs, including propagation characteristics and medium access control protocols for medical implant communication service (MICS) band, industrial scientific and medical (ISM) band, wireless medical telemetry band (WMTB) and ultra-wideband (UWB). But there are still many challenges in body area networks (BANs), which call for increasing mobility, higher capacity and lower power consumption. In order to design better wireless devices for health care applications, it is significant to understand the propagation characteristics in BANs. Furthermore, understanding the performance of on-body communication links is also important in designing and evaluating medium access control protocols for specific scenarios defined in [25].

With wireless sensors placed on a person, the human body motions could be accurately recognized and remotely detected. In BANs, temporal variations of channel are related to body conditions, body motions, antenna positions, frequency bands and surrounding environment. The general characterization of on-body fading channels is required to be analyzed thoroughly in a scenario based approach [21]. Among all the influenced factors mentioned above, the human body motion is a key factor leading to a greater variation of the communication channel. This paper

presents a quantitative approach to describe different human body motions from the narrowband measurement.

A measurement champaign has been performed with regard to fading effects caused by body movements. Studies of propagation characteristics for these dynamic channels have been done in indoor environment around 868 MHz, 2.4 GHz and 5 GHz [1, 2, 3, 7, 16, 17, 18]. The considered frequency bands include MICS band, ISM band, WMTB band and UWB band. Measurements related to dynamic channels were conducted in anechoic chamber, office room and hospital room by either channel sounder in wideband or vector network analyzer (VNA) in narrowband. Some of past researches are analysis of on-body propagation effects, including the modeling of path loss (PL) model [13, 12] for a variety of scenarios at 400 MHz, 600 MHz, 900 MHz, 2.4 GHz, and UWB bands. Some previous papers are concentrated on statistical characterization of channels for a given scenario by attaching a probability density function (pdf) [16], where Log-normal, Weibull, Nakagami-*m* and Gamma distributions are considered to characterize on-body dynamic channels. Also cumulative distribution function (CDF) is analyzed, where Nakagami-*m* distribution is used to model channels that incorporate channel models at 868 MHz indoor. Other papers concentrated on analysis second-order temporal statistics [18] by indicating fading rate and fading duration from measurements. Additionally, discussion about channel temporal stability is readily given in [11, 19]. However, few of these papers describe the dynamic channels for human body motions in a quantitative and thorough method.

This paper focused on a thorough investigation of characteristics of on-body channel modeling, induced by continuous human body motions in the narrowband. Based on a scenario approach, the probability distribution and the second order statistics are measured and discussed case by case. Weibull distribution is considered as a suitable description of walking and jogging motions in most of the cases, while log-normal distribution is representative of standing motion in several cases. Doppler spread spectrum, RMS Doppler bandwidth and the shape of Doppler spread spectrum are measured and analyzed with a VNA. Doppler spread is the width of received spectrum when a single tone waveform has been transmitted, which provides information about the fading rate of the channel. And RMS Doppler bandwidth is used to describe the distribution of the power with respect to the Doppler spread. Doppler spread and RMS Doppler bandwidth are of great importance to determine the minimum signalling rate allowable for coherence demodulation and to improve detection and to optimize transmission at the physical layer. Coherence time, which is an equal description of Doppler spread in frequency domain, is analyzed in time domain.

The remainder of this paper is organized as follows. The measurement environment, measurement equipment and on-body to on-body measurement scenarios are described in Sect. 2. Section 3 presents a brief discussion of statistical distributions of amplitude variations for different scenarios. And corresponding second order statistics, including fading rate and fading duration, is given in Sect. 4. Section 5 shows the analysis of Doppler spread spectrum, including Doppler spreads, RMS Doppler spreads in frequency domain and coherence time in time domain. A set of time domain waveforms and frequency spectrums are shown visually to compare Doppler spreads for different human body motions. Finally, conclusions are drawn to summarize propagation characteristics of on-body channels for human body motions in BANs, which provide important parameters for designing medical devices.

2 Measurement Setup

The on-body to on-body channel measurements were performed by using two antennas placed on a test subject in a shielded room with a size of $2.32 \times 2.41 \times 2.29\ \mathrm{m}^3$ at Center for Wireless Information Network Studies lab of Worcester Polytechnic Institute. Three sets of antennas are used during the measurements, all of which are omnidirectional working at 400 MHz, 2.25 and 4.5 GHz within MICS, ISM and UWB bands. Antennas used for narrowband measurement at 400 MHz consist of a loop antenna as the receiver and a helical antenna as the transmitter; monopole antennas, working in a frequency band from 2.1 to 2.4 GHz, are designated to send a single tone waveform at 2.25 GHz from transmitter to receiver; and patch antennas (SkyCross^{TM} SMT-3TO10M-A) are proposed to send and to receive a single tone waveform at 4.5 GHz.

Short time channel gain variations were measured using Agilent E8363B VNA. A continuous single tone signal waveform at 400 MHz, 2.25 GHz, and 4.5 GHz with a transmission power of 0 dBm was generated respectively by Tx port of VNA in time domain. S21 Parameter, measured and stored in the PC in real time, was analyzed and evaluated off-line. In the 20 s interval, the network analyzer took samples of amplitudes of the received signal at the rate of 80 samples/s. Therefore the maximum Doppler shift measurable is 40 Hz, and resolution is 0.012 Hz.

All measurements were based on different motions, where transmitting and receiving antennas were attached to different positions of human body. Using a scenario-based approach [6], a scenario set, denoted by $S = \{Freq, Motion, TX, RX\}$, is composed of a frequency set *Freq*, a motion set *Motion*, two antenna position sets *TX* and *RX*. In the motion set, three different human movements have been measured: standing still, walking and jogging on a spot, denoted as $Motion = \{Stand, Walk, Jog\}$. Only respiration and palpitation exist when the human body is standing still.

For the walking cycle, the human body is walking with arms and feet moving slowly and repeatedly in a small range. When the human body is jogging, both arms and feet moved very quickly, which would cause greater channel fluctuation. The frequency set *Freq* is composed of *Freq* = {400 MHz, 2.25 GHz, 4.5 GHz}, where the increasing frequency of transmitters would have impact on small scale fading characteristics of body area network.

The transmitting and receiving antennas are placed at different positions on the test subject's body. The receiver is fixed at the right hip of the test subject which is denoted by $RX = \{RightHip\}$, since the coordinatior in the BANs is often considered as the center to receive data from other sensors in-body or on-body. And the location of transmitter is denoted as $TX = \{\text{Back, Chest, LeftWrist, LeftAnkle, RightAnkle}\}$. Figure 1a illustrates the lay-out of shielded room and Fig. 1b shows the locations of antennas on the tested subject.

3 First Order Statistical Characterization

According to different measurement scenarios, the statistical distributions of envelop fading are summarized for the scenario set *S*, where effects of human body motions, antenna positions, and transmission frequencies are all taken into account thoroughly in this section. The set *S* is defined as $S = \{\{Freq\}, \{Motion\}, \{TX\}, \{RX\}\}$, where *Freq* is the transmission center frequency, *Motion* is the human body motions, *TX* is the antenna position of transmitter, *RX* is the antenna position of the receiver. Rayleigh, Weibull, Nakagami-*m* and Log-normal distributions are considered as potential statistical models for path amplitude variations in time domain. Pdf of these four probabilistic distributions [14] are described below.

- Rayleigh distribution with pdf

$$f(x|\sigma) = \frac{x}{\sigma^2}\exp\left\{-\frac{x^2}{2\sigma^2}\right\}\ x \in \{0, +\infty\}, \tag{1}$$

where x is the envelope amplitude of received signal, σ^2 is the mean power of the received signal. Rayleigh distribution is considered as a reasonable envelop fading channel model of a received signal for mobile communication systems.

- Weibull distribution with pdf

$$f(x|\lambda, k) = \begin{cases} \frac{k}{\lambda}\left(\frac{x}{\lambda}\right)^{k-1}\exp\{-\left(\frac{x}{\lambda}\right)^k\}\ x \geq 0 \\ 0 \qquad\qquad \text{otherwise} \end{cases} \tag{2}$$

where x is the envelope amplitude of received signal, k is the shape factor, λ is the scale factor. Both the shape and scale factors are positive to characterize the Weibull distribution. The Weibull distribution is considered to show a good fit to experimental fading channel measurements in outdoor environments. Weibull distribution also exhibits a good fit for some cases on-body channel fading models.

- Nakagami-*m* distribution with pdf

$$f(x|m, \omega) = \frac{2m^m}{\Gamma(m)\omega^m}x^{2m-1}\exp\left\{-\frac{m}{\omega}x^2\right\}, \tag{3}$$

where $\Gamma(\cdot)$ is the Gamma function, x is the envelope amplitude of received signal, m is the shape factor and ω is a controlling speed. A special case is when $m = 1$, Nakagami-*m* fading performs similar as Rayleigh fading with an exponentially distributed power. Nakagami-*m* distribution is regarded as the best fit to some urban multipath measurements occasionally.

- Log-normal distribution pdf

$$f(x|\mu, \sigma) = \frac{1}{x\sigma\sqrt{2\pi}}\exp\{-\frac{(\ln x - \mu)^2}{2\sigma^2}\}\ x \in \{0, +\infty\}, \tag{4}$$

where x is the envelope amplitude of received signal, μ is the mean of distribution, and σ is the standard deviation of the Log-normal distribution.

In order to compare the goodness of statistical distribution fittings, we obtain the log likelihood ratio between the CDF of measurements and theoretical CDFs for Rayleigh, Weibull, Nakagami-*m* and Log-normal distributions. Figure 2 shows the CDF fittings for scenario set $S1 = \{\{2.25\ \text{GHz}\}, \{Jog\}, \{LeftAnkle\}, \{RightHip\}\}$. In this scenario, Weibull distribution has the maximum log likelihood ratio. Table 1 gives pdf parameters for the these distribution models fitted to the envelope of the received signal strength for scenario set *S*2 via the maximum log likelihood ratio, where *S*2 is defined as the set of $S2 = \{Freq2, Motion2, TX2, RX2\}$ and $Freq2 = \{2.25\ GHz\}$, $Motion2 = \{Stand, Walk, Jog\}$, , $TX2 = \{Chest, Back, LeftWrist, LeftAnkle, RightAnkle\}$ and $RX2 = \{RightHip\}$. For a total number of 15 measurements of scenario set *S*2, there are nine scenarios fitted into Weibull distribution. Log-normal distribution is the best fit for standing motion in several cases. Nakagami-*m* distribution is a good candidate for the statistical model for walking motion in several cases.

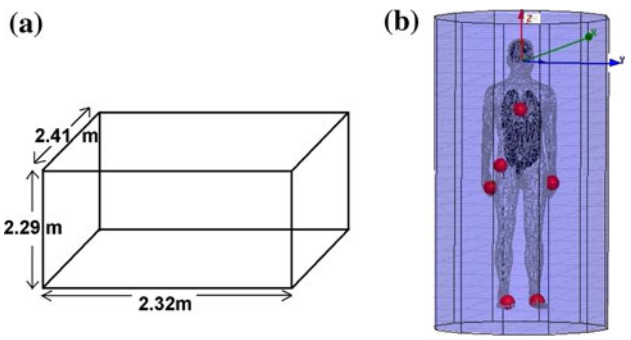

Fig. 1 **a** Shielded room, **b** antenna positions

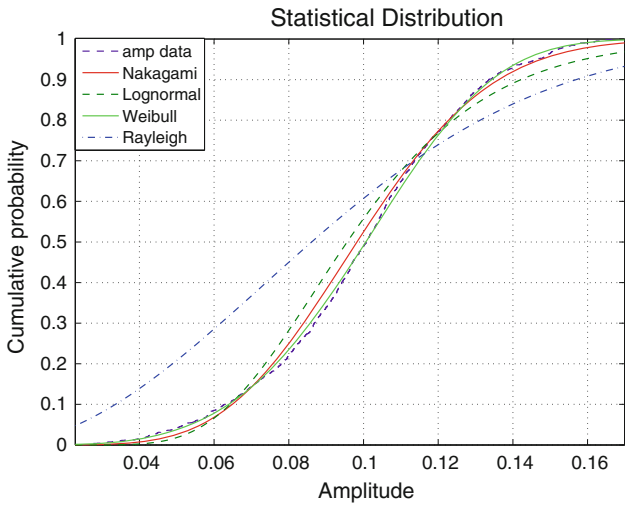

Fig. 2 Statistical distributions of envelope fading

Table 1 Statistic distributions

Motion	TX	Distribution	Parameter
Stand	Chest	Weibull	$\lambda = 0.18$, $k = 27.39$
	Back	Log-normal	$\mu = -1.7$, $\sigma = 0.025$
	Left wrist	Weibull	$\lambda = 0.11$, $k = 49.28$
	Left ankle	Log-normal	$\mu = -2.73$, $\sigma = 0.11$
	Right ankle	Log-normal	$\mu = -2.35$, $\sigma = 0.042$
Walk	Chest	Weibull	$\lambda = 0.15$, $k = 7.2$
	Back	Nakagami	$m = 10.39$, $\omega = 0.019$
	Left wrist	Nakagami	$m = 4.6$, $\omega = 0.01$
	Left ankle	Weibull	$\lambda = 0.12$, $k = 6.3$
	Right ankle	Weibull	$\lambda = 0.12$, $k = 4.05$
Jog	Chest	Weibull	$\lambda = 0.14$, $k = 5.26$
	Back	Weibull	$\lambda = 0.11$, $k = 4.24$
	Left wrist	Weibull	$\lambda = 0.15$, $k = 4.48$
	Left ankle	Weibull	$\lambda = 0.11$, $k = 4.15$
	Right ankle	Nakagami	$m = 3.5$, $\omega = 0.014$

4 Second Order Statistical Characterization

In BANs, different human body motions, antenna positions and center frequencies will result in shadow fading. And the received signal strength fluctuates extensively according to the characteristics of these channels. Given a certain threshold, the performance of the receiver is deteriorated due to the deep fading of channel, which will also give rise to a higher error rate. The statistics of level crossing (fade) rate and fade duration are the other two important parameters for designing medical sensors in BANs. Figure 3 describes the basic concept and parameters related to the level crossing rate and fading duration.

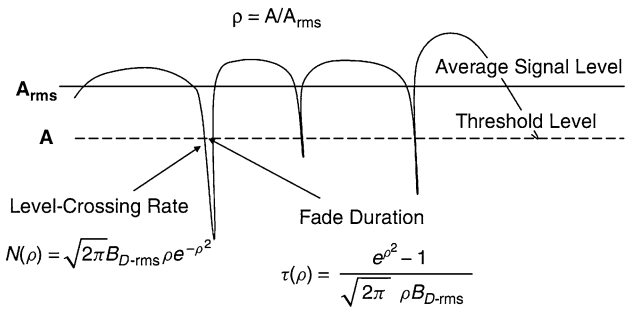

Fig. 3 Level crossing rate and fading rate

4.1 Level Crossing Rate

The level crossing rate is defined as the average number of downward crossings of a certain threshold T per second. The level crossing rate $N(\rho)$ is defined as

$$N(\rho) = \sqrt{2\pi} B_D \rho e^{-\rho^2} \tag{5}$$

From the definition, we got the normalized level crossing rate $N(\rho)$ versus normalized threshold ρ in decibels for scenario set $S2$ shown in Fig. 4, where $N(\rho)$ is normalized to the RMS value of the number of crossings and ρ is normalized to the RMS value of the envelope of the signal. For low values of normalized threshold ρ below -6 dB in this case, we rarely have a fade crossing this threshold. As the normalized threshold ρ increases, the number of fades crossing the threshold also increases until ρ is zeros, which means that the actual threshold reaches the RMS value of the envelope of the signal. For the three human motions defined in $S1$, the jogging motion had the greatest variation of channel fading with a peak value of 7.12 Hz. Communication links for walking has a less crossing rate, since it is not as intense as jogging and the channel suffers from less shadow fading across the normalized threshold ρ. As a result of relatively stable motion, the level crossing rate is the smallest for standing. Only a small number of fade crossings happen for a certain normalized threshold ρ.

4.2 Average Fade Duration

The average fade duration, also referred to as outage duration, is calculated as the average time duration when fading is below a certain threshold. The average fade duration $\tau(\rho)$ is defined as

$$\tau(\rho) = \frac{e^{\rho^2} - 1}{\sqrt{2\pi}\rho B_D} \tag{6}$$

Fig. 5 explicitly gives the average fade duration versus normalized threshold ρ for scenario set $S1$, which shows that the standing motion has the fastest increasing speed compared with walking and jogging motions. For a total measurement duration of 20 s, the average fade duration time is a

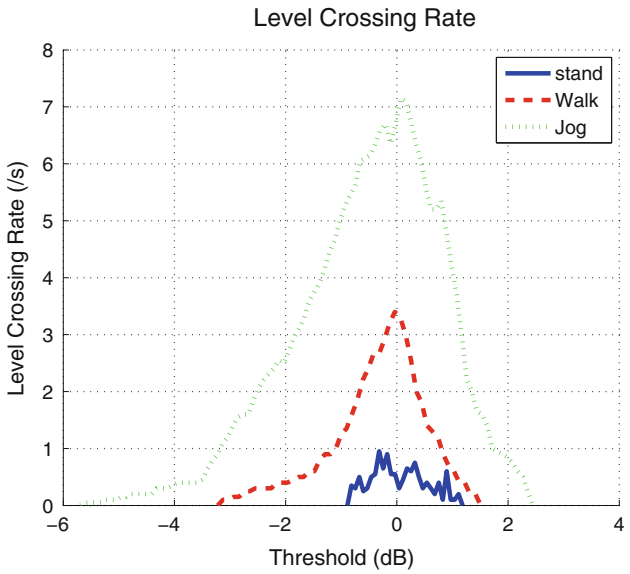

Fig. 4 Level crossing rate

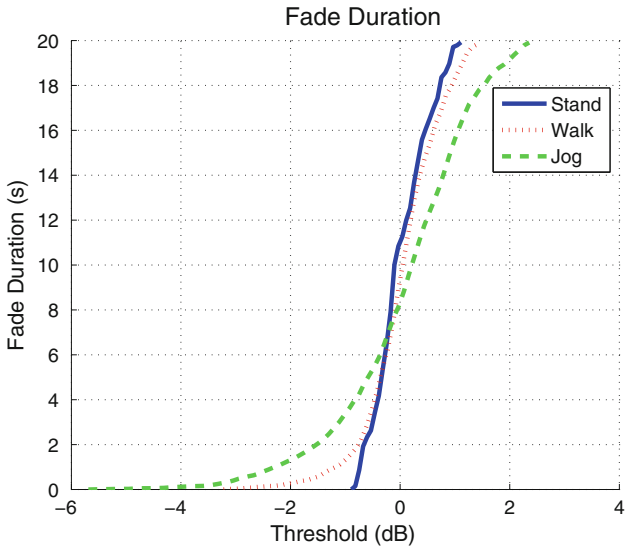

Fig. 5 Fade duration

non-decreasing function of the normalized threshold. For a lower values of $\rho 0$, there is almost no fading duration below the normalized threshold. As the normalized threshold increases, the fade duration keeps on rising until it reaches to the measurement time duration (20 s) as the normalized threshold arrives at its peak amplitude.

4.3 Outage Probability

For a given threshold, the outage probability is computed as the probability distribution of fading when the signal power drops below this threshold. It is a measure of the quality of transmission in a mobile radio channel. If the average number of downward crossings for a normalized level is denoted as $N(\rho)$ and the average fade duration is $\tau(\rho)$, then the outage probability is calculated as

$$Prob\{\alpha < \rho\} = \tau(\rho) \times N(\rho) \tag{7}$$

And the percentage of time that the system can send information is given as

$$S = 1 - Prob\{\alpha < \rho\} = 1 - \tau(\rho) \times N(\rho) \tag{8}$$

IEEE 802.15.6 standard [24] has proposed that the latency requirement is <125 ms for medical applications and 250 ms for non-medical applications. In order to satisfy these requirements, a higher normalized threshold, coming from PL model is claimed to maintain the throughput of the unstable channel in packet communications.

5 Doppler Spread and Coherence Time Analysis

5.1 Doppler Spread

It is well known from the analysis of electromagnetic signals that if there is a relative motion between the source and the receiver, an apparent change will occur in frequency between the source of a wave and the receiver of the wave. If either the source or the receiver both move towards the other, the receiver will perceive a higher frequency. This is because the receiver will receive a greater number of electromagnetic waves per second and interpret the greater number of waves as a higher frequency. Conversely, if the source and the receiver are moving apart, the receiver will receive a smaller number of electromagnetic waves per second and will perceive a lower frequency. In both cases, the frequency produced by the source will remain constant. The maximum Doppler frequency shift is determined by the velocity of the movement v_m and the length of propagation wave $\lambda = \frac{c}{f_c}$ by

$$\pm f_m = \frac{v_m}{\lambda} \tag{9}$$

where c is the propagation velocity and f_c is the transmitting frequency. When the transmitter is moving toward the receiver, the Doppler frequency shift f_m would be positive. On the other hand, f_m would be negative if transmitter moves away from the receiver. Hence, the maximum value of f_m could be approximate from Doppler spread B_D of the on-body to on-body communication.

From the NarrowBand measurement results, we have the time domain response $H(f_c; t)$ received from an unmodulated sine wave transmitted at 400 MHz, 2.25 GHz and 4.5 GHz respectively. By design, each measurement is a

sample of an ergodic process and stationary. All the following analysis below assumes that the channel is wide-sense stationary at a minimum [10].

Applied a threshold of -10 dBm in the frequency domain, Doppler spread $D(\lambda)$ could be derived from the Fourier transform of the time domain data $H(f_c; t)$, where $D(\lambda) = \int_{-\infty}^{\infty} H(f_c; t)e^{-j2\pi\lambda t}dt$. A set of Doppler spreads for a specific scenario $S3 = \{Freq3, Motion3, TX3, RX3\}$ is shown in Fig. 6, including both time domain response $H(f_c; t)$ and corresponding response $D(\lambda)$ in frequency domain. In this specific case, we have $Freq3 = \{2.25\ \text{GHz}\}$, $Motion3 = \{Stand, Walk, Jog\}$, $TX3 = \{LeftAnkle\}$ and $RX3 = \{RightHip\}$. The Doppler spreads for standing, walking and jogging motions are approximately 0.6758 Hz, 2.929 Hz and 11.19 Hz for the communication link between left ankle and right hip.

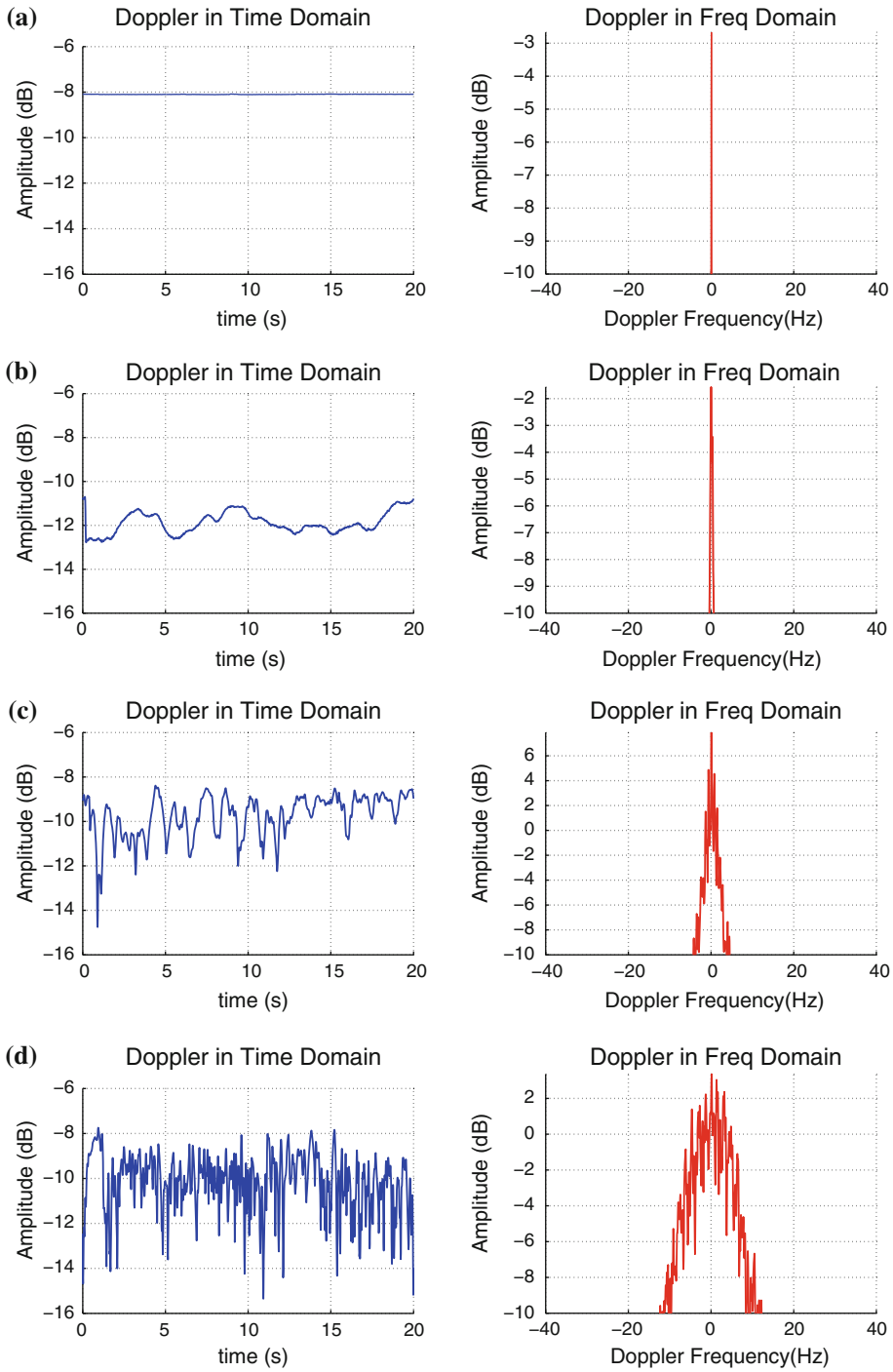

Fig. 6 Doppler spread in time domain and frequency domain for different human body motions at 2.25 GHz. **a** Freespace, **b** stand still, **c** walk on a spot, **d** run on a spot

Table 2 Doppler spreads and RMS Doppler bandwidth for human body motions at different transmission range at 2.25 GHz

Motion	*TX*	Doppler spread (Hz)	RMS bandwidth (Hz)
Stand	Chest	0.826	0.8673
	Back	0.876	0.776
	Left wrist	0.826	0.698
	Left ankle	0.676	0.7696
	Right ankle	0.727	0.983
Walk	Chest	4.781	1.899
	Back	4.981	2.209
	Left wrist	4.481	2.061
	Left ankle	2.929	1.879
	Right ankle	4.281	2.006
Jog	Chest	9.937	2.898
	Back	9.287	2.728
	Left wrist	9.587	3.115
	Left ankle	11.190	3.008
	Right ankle	10.690	3.184

Table 3 Doppler spreads and RMS Doppler bandwidth for human body motions at different transmission frequency

TX	Freq	Doppler spread (Hz)	RMS Doppler bandwidth (Hz)
Left ankle	400 MHz	1.977	1.4476
	2.25 GHz	2.929	1.8789
	4.5 GHz	3.029	1.9861

For the on-body to on-body measurements, Doppler spread varies approximately from 0.6 to 11 Hz for scenario set *S*3, which is composed of a frequency set *Freq*, a motions set *Motion* and antenna position sets *TX* and *RX*. Table 2 lists Doppler spreads for a specific scenario set *S*2 defined in Sect. 3. From Table 2 we can conclude that Doppler spread increases from 0.676 to 11.190 Hz as the motions of human body changes and antenna positions change. And as the transmission range which is related to positions of TX antenna, Doppler spreads also rises in a small range when the distance between RX and TX increases. Table 3 lists Doppler spreads based on a scenario set $S4 = \{Freq4, Motion4, TX4, RX4\}$, where $Motion4 = \{Walk\}$, $Freq4 = \{400\ \text{MHz}, 2.25\ \text{GHz}, 4.5\ \text{GHz}\}$, $TX4 = \{LeftAnkle\}$ and $RX4 = \{RightHip\}$. From Table 3, it is easy to come to the conclusion that Doppler spread increases with respect to the center frequency of transmission waveform for the same antenna position of transmitter and receiver. The Doppler spread rises along with the center frequency of transmission waveform.

5.2 RMS Doppler spread

A more specific estimation of Doppler spread is the RMS Doppler bandwidth [10] defined by

$$f_N = \left[\frac{\int \lambda^2 V(\lambda) d\lambda}{\int V(\lambda) d\lambda}\right]^{1/2}, \tag{10}$$

where $V(\lambda)$ is the Fourier transform of the complex auto-correlation function of $H(f_c; t)$. RMS Doppler bandwidth is proposed to describe Doppler shift by calculating the weighted signal power rather than a simply overall width of the spectrum in a more scientific method.

For the scenario set *S*, the RMS Doppler bandwidth changes in a range of 0.698–3.184 Hz, where difference comes from various human body motions, center waveform frequency, and antenna positions on the test subject. In Table 2, for the standing still motion, RMS Doppler bandwidth is always below one, which shows a concentrated distribution of signal power. While for walking and jogging motions, RMS Doppler bandwidth is much larger than that of standing still, since signal power is dispersedly distributed in the frequency domain. Doppler spread spectrums in Fig. 6 have shown an example of power distribution in frequency domain, where the Doppler Spread increases from (b) to (c) to (d). For a specific scenario *S*4, Table 3 illustrated that RMS Doppler spread bandwidth also increases with respect to the center frequency of transmission signal for the same transmitting and receiving antenna positions, but not proportionally.

5.3 Shape of Doppler Spread Spectrum

In the on-body to on-body channel, the transmitter and receiver could be either stationary or mobile. The relative mobility will lead to different Doppler shapes in frequency domain, where the "Bell-Shaped" Doppler spectrum are relative to center frequency and human body motions. In this study, we obtained maximum likelihood estimates of received signal strength in dB related to frequency variations of three curves, which is used to characterize and model channels in past researches.

- Laplacian

$$F(f_0) = \frac{a}{b + cf_0^2} + d, \tag{11}$$

where $f_0 = \frac{f}{f_c}$, and f_c is the center frequency of transmission.

- Gaussian

$$F(f_0) = \sum_{i=0}^{i=n-1} a_i \exp(-(f_0 - f_i)^2 / c_i^2), \tag{12}$$

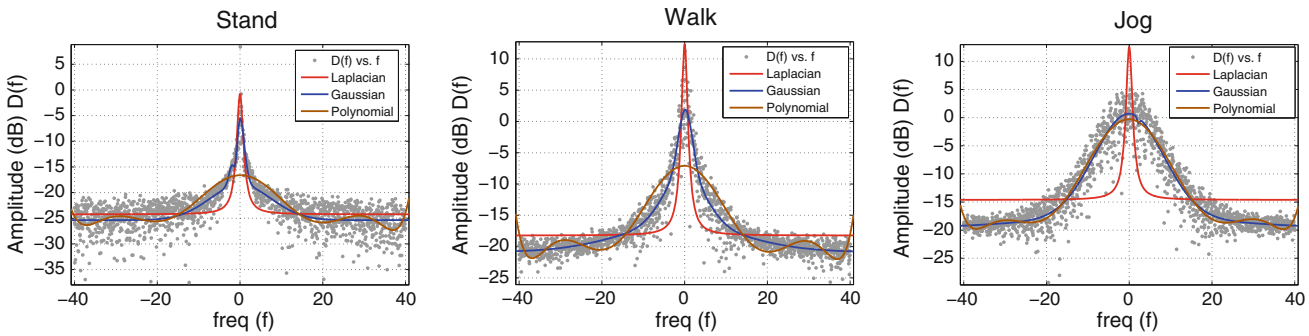

Fig. 7 Shape of Doppler spread spectrum for different human body motions at 2.25 GHz

this is an nth order Gaussian model, where $f_0 = \frac{f}{f_c}$, and f_c is the center frequency of transmission.

- Polynomial

$$F(f_0) = \sum_{i=0}^{i=n-1} p_i f_0^i, \tag{13}$$

this is an nth order Polynomial model, where $f_0 = \frac{f}{f_c}$, and f_c is the center frequency of transmission.

In order to compare goodness of the three curve fittings, we consider root mean square error (RMSE) between these curves and actual measured data. Given total deviation of measured values with the fit to the measured values, we come to estimation of standard deviation of random component in measured data, and is defined as

$$\text{RMSE} = \sqrt{\text{MSE}(\hat{\theta})} = \sqrt{E((\hat{\theta} - \theta)^2)}, \tag{14}$$

where $\hat{\theta}$ is an estimator with respect to the measured data θ leading to the least RMSE value. Comparing the RMSE for Laplacian, Gaussian and Polynomial estimators, we could conclude that the 4th Gaussian function is a good candidate for a jogging motion. But it does not always perform better than Laplacian and Polynomial estimators for standing and walking motions. There are only 8 out of 75 cases where the Laplacian estimator outperforms the 4th Gaussian estimator for the scenario S. Yet, Laplacian estimator is usually a poor fitting of the power amplitude of jogging motion. Figure 7 shows a sample of curve fittings for scenario $S3$, where the 4th Gaussian estimator shows a better performance than Laplacian and Polynomial estimators.

5.4 Coherence Time

Coherence time is the description of time dispersive nature of the channel in time domain, equivalent to Doppler spread in frequency domain. It is actually a statistical measurement of the time duration over which the channel impulse response is essentially invariant. In other words, coherence time is the time duration over which two received signal has a strong amplitude correlation. In a baseband transmission, a distortion will occur when bandwidth of the signal is greater than the inverse of coherence time. Coherence time and Doppler spread are inversely proportional to each other.

$$f_m = \frac{c}{T_c}, \tag{15}$$

where c is a constant value. Channel coherence time is typically defined as the time duration over which the normalized auto correlation coefficients of time domain data is above 0.5, defined by

$$\rho(m) = \frac{\sum_{n=1}^{N-|m|} \{x(n+m) - m_x\}\{x^*(n) - m_x\}}{|r(n+m)| \times |r(n)|}, \tag{16}$$

where m_x is the mean value with $m_x = \frac{1}{N}\sum_{n=1}^{N} x(i)$, and $|r(n)| = \sum_{n=1}^{N} \{x(n) - m_x\}^2$. The correlation function for scenario $S3$ is shown in Fig. 8.

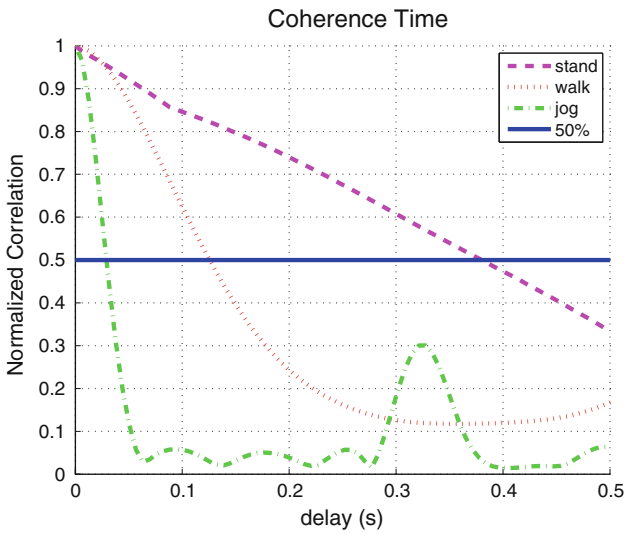

Fig. 8 Coherence time analysis for different human body motions

Hence, the coherence time for $S3$ is 125.1 ms, which means that a maximum symbol transmission rate of $\frac{1}{T_c} = 8$Hz is required to avoid distortion from frequency dispersion in digital communication system.

6 Conclusion

Using wireless sensors around the human body to continuously monitor human movements is a promising new application in BANs. In this paper, we describe a comprehensive measurement and modeling champaign in MICS, ISM and UWB bands that characterized the statistical distribution and Doppler spreads for different human body motions. The center frequency, antenna positions will also have impacts on the statistical distribution and Doppler spreads. The case-by-case analysis shows that it is hard to merge the characterization of the human body motions into a unique case. For most of the cases, Weibull distribution is a good candidate for the general dynamic channel model. The second order statistics, Doppler spread and coherence time provide a quantitative description of different human body motions in BANs.

References

1. S. L. Cotton, G. A. Conway, and W. G. Scanlon, A time-domain approach to the analysis and modeling of on-body propagation characteristics using synchronized measurements at 2.45 GHz, *IEEE Transactions on Antennas and Propagation*, Vol. 57, No. 4, pp. 943, 2009.
2. S. L. Cotton, and W. G. Scanlon, Characterization and modeling of the indoor radio channel at 868 MHz for a mobile bodyworn wireless personal area network, *IEEE Antennas and Wireless Propagation Letters*, Vol. 6, pp. 51–55, 2007.
3. S. L. Cotton, and W. G. Scanlon, Characterization and modeling of on-body spatial diversity within indoor environments at 868 MHz, *IEEE Transactions on Wireless Communications*, Vol. 8, No. 1, pp. 14–18, 2009.
4. D. Cypher, N. Chevrollier, N. Montavont, and N. Golmie, Prevailing over wires in healthcare environments: benefits and challenges, *IEEE Communications Magazine*, Vol. 44, No. 4, pp. 56, 2006.
5. A. G. Dimakis, V. Prabhakaran, and K. Ramchandran, Fading results from narrowband measurements of the indoor radio channel. *Symposium on Information Processing in Sensor Networks, IPSN*, Los Angeles, pp. 111–117, 2005.
6. R. D. Errico, L. Ouvry, A statistical model for on-body dynamic channels, *International Journal of Wireless Information Networks*, Vol. 17, pp. 92–104, 2010.
7. A. Fort, C. Desset, P. De Doncker, P. Wambacq, and L. Van Biesen, An ultra-wideband body area propagation channel model-from statistics to implementation, *IEEE Transactions on Antennas and Propagation*, Vol. 54, No. 4, pp. 1820, 2006.
8. A. Fort, C. Desset, P. Wambacq, and L. V. Biesen, Indoor body-area channel model for narrowband communications, *IET Microwaves, Antennas and Propagation*, Vol. 1, pp. 1197, 2007.
9. R. Ganesh, and K. Pahlavan, Statistical modelling and computer simulation of indoor radio channel, *IEEE Proceedings Communications*, Vol. 138, No. 3, pp. 153, 2002.
10. S. J. Howard, and K. Pahlavan, Fading results from narrowband measurements of the indoor radio channel. *Proceedings of Personal, Indoor and Mobile Radio Communications*, London, pp. 92, 1991.
11. Z. Jian, D. B. Smith, L. W. Hanlen, D. Miniutti, D. Rodda, B. Gilbert, Stability of narrowband dynamic body area channel. *IET Microwaves, Antennas and Propagation*, Vol. 8, pp. 53–56, 2009.
12. N. Katayama, K. Takizawa, T. Aoyagi, J.-I. Takada, Li Huan-Bang, R. Kohno, Channel model on various frequency bands for wearable body area network, *International symposium on Applied Sciences on Biomedical and Communication Technologies*, Aalborg, pp. 1–5, 2008.
13. L. Lingfeng, P. De Doncker, and C. Oestges, Fading correlation measurement and modeling on the front side of a human body. *European Conference on Antennas and Propagation—EuCAP*, Berlin, pp. 969, 2009.
14. K. Pahlavan and A. H. Levesque, Wireless information networks, Wiley-Interscience, Sept. 2005.
15. K. Sayrafian-Pour, W. -B. Yang, J. Hagedorn, J. Terrill, and K. Y. Yazdandoost, A statistical path loss model for medical implant communication channels. *Proceedings of IEEE Personal, Indoor and Mobile Radio Communications*, Tokyo, pp. 2995–2999, 2009.
16. D. Smith, L. Hanlen, D. Miniutti, J. Zhang, D. Rodda, and B. Gilbert, Statistical characterization of the dynamic narrowband body area channel, *Applied Sciences on Biomedical and Communication Technologies*, pp. 1–5, 2008.
17. D. Smith, L. Hanlen, J. Zhang, D. Miniutti, D. Rodda, and B. Gilbert, Characterization of the dynamic narrowband on-body to off-body area channel. *Proceedings of IEEE International Conference on Communications, ICC '09*, Dresden, pp. 14–18, 2009.
18. D. Smith, D. Miniutti, L. Hanlen, D. Rodda and B. Gilbert, Dynamic narrowband body area communications: link-margin based performance analysis and second-order temporal statistics. *Proceedings of the IEEE Conference on Wireless Communications and Networking*, Sydney, pp. 14–18, 2010.
19. D. B. Smith, J. Zhang, L. W. Hanlen, D. Miniutti, D. Rodda, and B. Gilbert, Temporal correlation of the dynamic on-body area radio channel, *Electronics Letters*, vol. 45, pp. 1212, 2009.
20. S. Stein, Fading channel issues in system engineering, selected areas in communications, *IEEE Journal on Communications*, Vol. 5, No. 2, pp. 68, 2003.
21. H. Yang, A. Alomainy, Z. Yan, C. G. Parini, Y. Nechayev, P. Hall, and C. C. Constantinou, statistical and deterministic modelling of radio propagation channels in WBAN at 2.45 GHz. *Proceedings of IEEE Antennas and Propagation Society International Symposium*, Baltimore, pp. 2169, 2006.
22. B. Zhen, M. Kim, J. Takada, and R. Kohno, Characterization and modeling of dynamic on-body propagation. *ICST Conference on Pervasive Computing Technologies for Healthcare*, London, pp. 1, 2009.
23. B. Zhen, M. Kim, J. Takada, and R. Kohno, Finite-state markov model for on-body channels with human movements. *Proceedings of IEEE International Conference on Communications, ICC 2010*, Cape Town, pp. 1, 2010.
24. B. Zhen, M. Patel, S. Lee, and E. Won, Body area network (BAN) technical requirements, 15-08-0037-01-0006-ieee-802-15-6-technical-requirements-document-v-4-0.
25. Kamya Yekeh Yazdandoost, Kamran Sayrafian-Pour, 15-08-0780-09-0006-tg6-channel-model, April 2009.

Author Biographies

Ruijun Fu is a Master student in the Department of Electrical and Computer Engineering at Worcester Polytechnic Institute (WPI). She received her B.S. from Xi'an Jiaotong University, Xi'an, China in 2009. Her research interests include channel modeling in narrowband and wideband, human motions detection and localization algorithms in Body Area Networks.

Yunxing Ye is a PhD student in the Department of Electrical and Computer Engineering at Worcester Polytechnic Institute (WPI). He received his B.S. degree in electrical engineering from Zhejiang University, Hangzhou, China, and M.S. degree in electrical and computer engineering from WPI. His current research interests include cooperative robot localization and implant body area network localization technique.

Kaveh Pahlavan (PhD), is a Professor of Electrical and Computer Engineering, a Professor of Computer Science, and Director of the Center for Wireless Information Network Studies, Worcester Polytechnic Institute, Worcester, Massachusetts. His current area of research is wireless access and localization for body area networks and indoor geolocation and tracking for multi-Robot applications. His research background is on radio propagation modeling, modulation, channel coding and adaptive signal processing for digital communication over voice-band and fading multipath radio channels. He has contributed to numerous seminal technical and visionary publications and patents in voice-band modem, wireless LAN, wireless heterogeneous network, wireless indoor Geolocation and WiFi localization.